Dynamic adhesions and MARCKS in melanoma cells

Adriana Estrada-Bernal[1], Jesse C. Gatlin[2], Somkiat Sunpaweravong[3] and Karl H. Pfenninger[1,*]

[1]Department of Pediatrics and Department of Cell and Developmental Biology, University of Colorado School of Medicine, University of Colorado Cancer Center, and Colorado Intellectual and Developmental Disabilities Research Center, Aurora, CO 80045, USA
[2]Department of Biology, University of North Carolina, Chapel Hill, NC 27599, USA
[3]Department of Surgery, Songklanagarind Hospital, Prince of Songkla University, Songkla, Thailand
*Author for correspondence (e-mail: karl.pfenninger@ucdenver.edu)

Accepted 23 March 2009
Journal of Cell Science 122, 2300-2310 Published by The Company of Biologists 2009
doi:10.1242/jcs.047860

Summary

Cell motility necessitates the rapid formation and disassembly of cell adhesions. We have studied adhesions in a highly motile melanoma cell line using various biochemical approaches and microscopic techniques to image close adhesions. We report that WM-1617 melanoma cells contain at least two types of close adhesion: classic focal adhesions and more extensive, irregularly shaped adhesions that tend to occur along lamellipodial edges. In contrast to focal adhesions, these latter adhesions are highly dynamic and can be disassembled rapidly via protein kinase C (PKC) activation (e.g. by eicosanoid) and MARCKS phosphorylation. MARCKS overexpression, however, greatly increases the area of close adhesions and renders them largely refractory to PKC stimulation. This indicates that nonphosphorylated MARCKS is an adhesion stabilizer. Unlike focal adhesions, the dynamic adhesions contain α3 integrin and MARCKS, but they do not contain the focal adhesion marker vinculin. Overall, these results begin to define the molecular and functional properties of dynamic close adhesions involved in cell motility.

Key words: Cell adhesion, Integrins, MARCKS, Motility

Introduction

Motility enables metastatic cancer cells to migrate rapidly and invade the surrounding matrix (Pinner and Sahai, 2008). This translocation depends on coordinated regulation of the actin cytoskeleton and cell adhesion. The leading edge of the cell must form adhesions so that traction forces can work against the substratum (Broussard et al., 2008; Lock et al., 2008; Webb et al., 2002). To maintain their distal position, these adhesions must be turned over rapidly as the leading edge advances. Therefore, we will refer to them as 'dynamic adhesions'. However, the composition and regulation of these adhesions are not well understood.

Cell adhesion and migration on extracellular matrix (ECM) depend on integrins, heterodimeric transmembrane proteins that link ECM components, such as laminin, to the cytoskeleton. The cytoplasmic tails of integrins can interact with several adaptor and signaling proteins (Hynes, 2002; Luo and Springer, 2006; Takada et al., 2007). Once bound to an extracellular ligand, integrins generate an intracellular signal; conversely, their affinity can be regulated from within the cell (Hynes, 2002; Takada et al., 2007).

The participation of myristoylated alanine-rich C-kinase substrate (MARCKS) in cell adhesion and motility is known (Disatnik et al., 2004; Gatlin et al., 2006; Li et al., 1996; Manenti et al., 1997). MARCKS is a widely distributed peripheral membrane protein that binds calmodulin and actin and is found at the adherent surface of lamellipodia (Rosen et al., 1990). It contains two conserved regions involved in membrane association: a myristoylation and a phosphorylation domain. An unidentified additional domain targets the nonphosphorylated protein to adhesions (Gatlin et al., 2006). PKC-mediated phosphorylation of serine residues decreases MARCKS affinity for the plasma membrane and causes its translocation to the cytosol (Kim et al., 1994; McLaughlin and Aderem, 1995; Thelen et al., 1991).

In recent years, adhesions have been classified based on their composition and morphology (Lock et al., 2008; Webb et al., 2002; Worth and Parsons, 2008). Among them, focal adhesions are the best characterized by far. However, they inhibit migration rather than being a part of the mechanism of locomotion (Burridge et al., 1988; Izzard and Lochner, 1976; Lee and Jacobson, 1997). Dynamic adhesions, the subject of this report, most closely relate to focal complexes. These are small, transient structures seen immediately behind the leading edge of spreading or migrating cells (Lock et al., 2008; Webb et al., 2002; Worth and Parsons, 2008). They are often viewed as precursors of focal adhesions (Webb et al., 2003; Webb et al., 2002; Worth and Parsons, 2008).

The goal of the present study was to examine and characterize dynamic adhesions in highly motile cell lines (the metastatic melanomas, WM1617 and B16; glioblastoma, 10-08) by investigating the role of MARCKS in the regulation of adhesion and pseudopod attachment and detachment. We found that dynamic adhesions are not precursors of, or related to, the vinculin-containing focal adhesions, but instead contain MARCKS, which stabilizes them.

Results

Melanoma cell adhesions and the effect of exogenous 12(S)-HETE

To observe adhesions in spreading and locomoting melanoma cells we plated cells on laminin-coated glass coverslips and imaged them by interference reflection microscopy (IRM). This method reveals close adhesions as dark areas, whereas wider contacts are brighter than background (Izzard and Lochner, 1976). Fig. 1A shows an IRM sequence of a large cellular process (mouse B16 melanoma cell). Proximally, a set of characteristic, elongated and very dark structures were more or less radially arranged relative to the cell center – these were focal adhesions (Fig. 1A, black arrow). Focal adhesions did

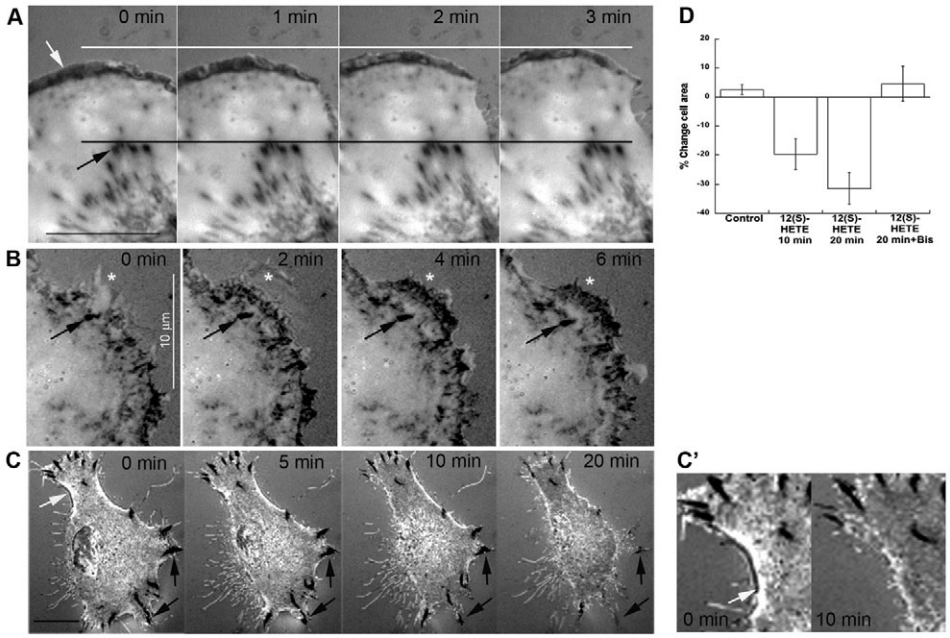

Fig. 1. IRM images of close contacts in live melanoma cells. (A) Distal lamellipodium of a B16 melanoma cell. A ribbon-like dynamic adhesion (white arrow) along the leading edge and a group of focal adhesions (black arrow) are evident. White and black lines are stationary. (B) Leading edge of a WM-1617 melanoma cell. A focal adhesion is marked with a black arrow. The white asterisk indicates an advancing lamellipodium and formation of a ribbon of close adhesions. (C) Effect of 12(S)-HETE (10^{-8} M), applied as a gradient, on melanoma adhesions and attached cell area. White arrow indicates a dynamic adhesion at the cell edge. It disappears after just over 5 minutes of 12(S)-HETE application. Black arrows indicate focal adhesions. (C') High magnification detail of C. Images were recorded at the indicated times. Scale bars: 10 µm. (D) Percentage change in cell area induced by 12(S)-HETE treatment with or without 10 nM bis-indolyl maleimide I (Bis), determined by measurement of the same cells before and after challenge. Values are means ± s.e.m. (n=10).

not move during the observation period. In the periphery of the lamellipodium, another, morphologically distinct type of close adhesion was visible. This large, ribbon-like structure closely followed the cell edge and moved rapidly relative to the white reference line. As the leading edge of the adhesion advanced its proximal rim was disassembled, resulting in net translocation of the adhesive ribbon. The advancing ribbon did not leave any adhesive structures behind except for a few dense puncta, which disappeared as one moved closer to the focal adhesions. Adhesive ribbons were also present along the leading edge of other cancer cells. Fig. 1B shows an immobile focal adhesion (arrow) as well as closely packed adhesive spots forming an irregular ribbon along the leading edge of a human melanoma cell (WM-1617). This ribbon moved away from the focal adhesion. Thus, highly dynamic adhesions are present at the leading edges of different cell types.

Previous studies have shown that some adhesions are sensitive to the intracellular messenger 12(S)-hydroxyeicosatetraenoic acid [12(S)-HETE] (Gatlin et al., 2006; Szekeres et al., 2002; Tang et al., 1995). To test the effect of this eicosanoid on cell adhesion, we exposed individual cultured cells (WM-1617) to gradients of 12(S)-HETE (pipette tip located 100 µm away, near the upper left hand corner in Fig. 1C) and imaged them over time by IRM.

Before eicosanoid application WM-1617 cells appeared spread out and exhibited multiple focal adhesions (Fig. 1C, black arrows). 12(S)-HETE gradient application caused the cell to contract, primarily on the left side, leaving behind several retraction fibers. They remained attached for some time, mostly via contacts that were brighter than background. Although close contacts other than focal adhesions disappeared rapidly (white arrow in Fig. 1C,C'), focal adhesions (black arrows) persisted much longer. However, they had also started to dissociate by 20 minutes. As a measure of cell adhesion, we determined cell contact areas using IRM before and after control or 12(S)-HETE challenge (Fig. 1D). The eicosanoid induced a highly significant decrease in attached cell area of about 20% within the first 10 minutes of exposure (P<0.005; n=10) and of over 30% after a total incubation time of 20 minutes (P<0.0005; n=10).

Because 12(S)-HETE acts via PKCε in growth cones, we assessed the effect of 12(S)-HETE on cell contact area after pre-incubation for 10 minutes with 10 nM bis-indolyl maleimide I (Bis), a selective inhibitor of PKCα, PKCβ and PKCε (Toullec et al., 1991). Bis completely inhibited 12(S)-HETE-induced reduction in adherent cell area [relative to 20 minutes of 12(S)-HETE, P<0.0005; n=10; Fig. 1D]. These results indicate that 12(S)-HETE triggers rapid detachment of non-focal contacts in WM-1617 melanoma cells via a Bis-sensitive, thus PKC-dependent, mechanism.

PKC isoforms, activation by 12(S)-HETE and PKC substrates

12(S)-HETE, directly and selectively activates PKCε in nerve growth cones (Mikule et al., 2003). Therefore, we screened WM-1617 cells for PKC isoforms. Fig. 2 shows western blots of equal amounts of WM-1617 protein probed with isoform-specific PKC antibodies. The most prominent isoforms were PKCε and PKCι. PKCλ, PKCα and PKCδ were less abundant but clearly present, whereas PKCβ and PKCθ were barely visible. PKCγ and PKCη were not detectable.

Next, we examined the activation and major substrates of PKC. WM-1617 cells were permeabilized and phosphorylation assays carried out. After phosphorylation, we collected sequentially the cytosolic supernatant, a Triton-X-100-soluble extract of the cell ghosts, and the Triton-insoluble fraction for gel electrophoresis and storage phosphor imaging. The representative images in Fig. 3A indicate that the major phosphopolypeptides were present almost exclusively in the cytosolic fraction. In terms of radiolabeled bands, the Triton extract appeared to consist mainly of a small residue of the cytosolic fraction. The Triton-resistant fraction exhibited numerous but relatively minor bands, and 12(S)-HETE, phorbol 12-myristate 13-acetate (TPA) and Bis had only small effects on phosphorylation levels.

The cytosol contained one major band (or doublet) of about 80 kDa. The PKC inhibitor, Bis, almost completely inhibited phosphorylation of this band, whereas 12(S)-HETE and TPA stimulated it. The low-molecular-mass polypeptides of this gel were probed by western blot for lactate dehydrogenase (LDH) as a

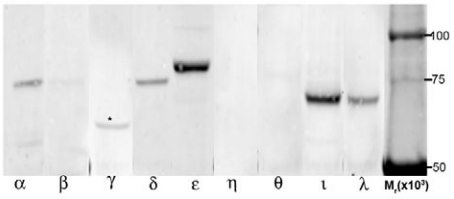

Fig. 2. PKC isoforms in WM-1617 cells. Total lysate of cultured WM-1617 cells (70 μg protein per lane) was subjected to immunoblot analysis using monoclonal antibodies selective for each PKC isoform. Asterisk indicates a crossreactive band that is not PKCγ. Blots for α, β, γ, δ, and ε came from one gel, and those for η, θ, ι and λ from another. M_r, apparent molecular mass.

cytosolic loading control. As Fig. 3A shows, sample loading was uniform, so that quantitative comparison of radiolabeling of the 80 kDa polypeptide was feasible. Quantitative results (percentage of change from control) are shown in Fig. 3B. Although TPA was a more potent activator, 12(S)-HETE nevertheless significantly increased phosphorylation of the 80 kDa polypeptide, by about 20%. Bis, alone or in conjunction with TPA or 12(S)-HETE, reduced phosphorylation levels by over 30% relative to control and by greater amounts relative to 12(S)-HETE or TPA.

Identification of MARCKS and phosphorylation-dependent MARCKS translocation

The apparent molecular mass, the stimulation of phosphorylation by 12(S)-HETE, as well as the cytosolic location, all suggested that the 80 kDa phosphopolypeptide was MARCKS (Aderem, 1995; Blackshear, 1993). This was tested by immunoprecipitation from the cytosolic fraction with an anti- MARCKS antibody (Fig. 3C). The storage phosphor image shows that the 80 kDa band resided exclusively in the supernatant in controls (without MARCKS-specific antibody), whereas the antibody precipitated it almost quantitatively. Therefore, most, if not all the 80 kDa phosphopolypeptide was MARCKS (recoveries of total labeled protein were not equal).

Phosphorylated MARCKS resided primarily in the cytosolic fraction. We wanted to confirm that MARCKS is translocated in phosphorylation-dependent manner from the plasma membrane to the cytosol (Kim et al., 1994; Thelen et al., 1991) rather than being phosphorylated in the cytosol. Using western blots instead of radiolabeling, we assayed for the distribution of MARCKS protein in a membrane pellet relative to the cytosol of WM-1617 cells, under different experimental conditions. A representative experiment is shown in Fig. 4A and quantitative data are shown in Fig. 4B. In control conditions, only about 20% of total MARCKS protein was detected in the cytosol. In the presence of Bis, this value was about 15%. Upon TPA stimulation, however, about 65% of MARCKS protein was in the cytosol. Similarly, 12(S)-HETE increased the amount of cytosolic MARCKS more than twofold relative to the control. These results demonstrate that MARCKS is the primary PKC substrate, and that 12(S)-HETE causes translocation of phosphorylated MARKS (MARCKS-*P*) from the membrane to the cytosol.

Function of MARCKS in WM-1617 melanoma cells

To study the role of MARCKS in melanoma cells, we performed gain-of-function experiments by overexpressing a fusion protein of MARCKS and enhanced green fluorescent protein (MARCKS-GFP). Because MARCKS is highly conserved between humans and rodents, we expressed rat MARCKS, which allowed us to assess expression with species-specific antibodies. Cells untransfected (control), transfected with GFP alone, or transfected with

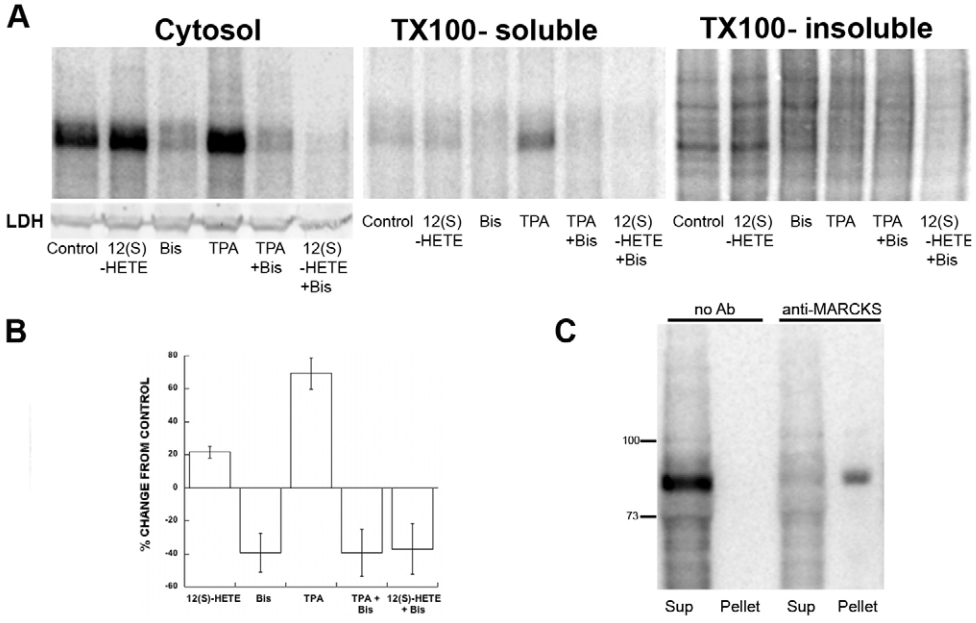

Fig. 3. PKC activation and substrates in WM-1617 cells. Permeabilized cells were incubated with the indicated effectors [10^{-8} M 12(S)-HETE, 1 μM TPA and/or 10 nM Bis] and with [^{32}P]ATP for 1 minute at 30°C. The culture supernatant was collected as the cytosol fraction. Subsequently, cells were lysed with 0.05% Triton X-100 and then solubilized with RIPA to prepare the TX100-soluble and the TX100-insoluble fractions, respectively. Equal amounts of cell protein were processed and analyzed for each experiment. (A) Storage phosphor images of SDS-polyacrylamide gels. Western blot of the cytosol gel shown above, probed with anti-LDH as a loading control, is shown on left hand side. (B) Quantitative analysis of the phosphor images of the 80 kDa polypeptide in the cytosolic fractions. Data are shown as mean (±s.e.m.) percentage change from control (n=3). (C) Phosphorylated cytosolic fraction of additional WM-1617 cells was used for immunoprecipitation with anti-MARCKS antibody. The phosphor image shows supernatants (Sup) and precipitates (Pellet) obtained with or without the antibody.

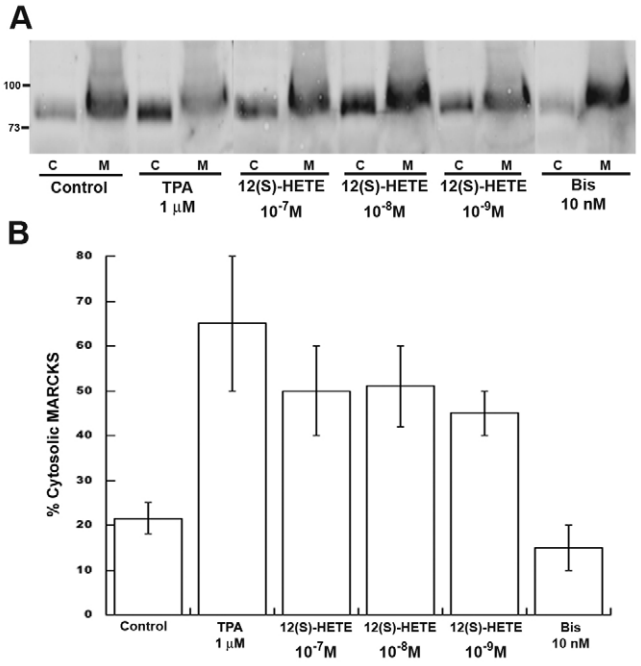

Fig. 4. Phosphorylation and translocation of MARCKS to the cytosol. Cells were treated with the indicated effectors for 10 minutes. After incubation, cultures were scraped off and spun to separate membranes plus cytoskeleton (M) from cytosol (C). (A) Western blot of fractions probed with anti-MARCKS antibody. (B) Quantitative analysis of MARCKS translocation to the cytosol, expressed as percentage of MARCKS in the cytosol over total cellular MARCKS immunoreactivity (averages ± s.e.m.; n=3).

MARCKS-GFP were lysed and western blots prepared. In Fig. 5A,B, blots were probed with anti-rat and anti-human MARCKS, respectively. Although expression levels of endogenous (human) MARCKS were the same for all three samples (B), the anti-rat MARCKS antibody recognized a strong band only in the MARCKS-GFP transfectants, at a M_r reflecting the size of MARCKS plus GFP. The antibody was weakly crossreactive with human MARCKS (80 kDa). Because the relative affinities of the anti-rat and anti-human MARCKS antibodies are unknown, we can only estimate (assuming equal affinities) the increase in MARCKS expression in the transfectants. Densitometric analysis of the blots (Fig. 5A,B) suggested that this increase was about 4.5-fold. Blots from the same samples also were probed with anti-GFP, together with anti-actin as a loading control. At constant actin levels, GFP-only cells exhibited a strong band of the fluorescent marker, whereas MARCKS-GFP cells exhibited a band at 100 kDa (fusion protein; Fig. 5C). Weaker bands at about 75 kDa and 27 kDa were probably breakdown products of the fusion protein.

Cells transfected with MARCKS-GFP and GFP alone were examined by fluorescence microscopy and IRM (Fig. 5E,G). GFP alone exhibited a distribution pattern typical for a largely cytosolic protein (Fig. 5E): fluorescence intensity corresponded to cell thickness. MARCKS-GFP expression generated a quite different image (Fig. 5G). Edge fluorescence was enhanced, whereas labeling across the cell was uniform, except for perinuclear fluorescence. For quantitative analysis, we prepared intensity scans across cell processes (average length: 26.4±1.0 μm for GFP alone and 26.3±1.4 μm for MARCKS-GFP). Representative sample scans are shown. In Fig. 5F, the scan is roughly bell-shaped, as expected for a predominantly cytosolic protein; by contrast, Fig. 5H shows enhanced label near the cell perimeter. To analyze these scans quantitatively, profiles were normalized for intensity maxima (set to 50 arbitrary intensity units). We then determined for each normalized scan: (1) the separation between the two highest intensity peaks (in a bell-shaped profile, they result from data noise and are very close together, but they are widely separated if edge labeling is prevalent); and (2) the intensity in the middle between the maxima. This would be near the maximum for a bell-shaped curve, but significantly below in the case of edge labeling. The results (Fig. 5I) reveal quantitatively that GFP-only profiles were distinct from those for MARCKS-GFP, and that MARCKS-GFP was predominantly associated with the plasma membrane. MARCKS-GFP fluorescence also highlighted a large number of filopodial processes, which seemed to be lacking in GFP-only cells.

To confirm that overexpressed MARCKS was localized at the cell membrane, we used total internal reflection fluorescence (TIRF) microscopy. This technique enables examination of a zone, about 100 nm deep, and adjacent to the glass coverslip, that includes the intercellular space and adherent plasma membrane (Groves et al., 2008; Toomre and Manstein, 2001). We combined two different TIRF approaches: (1) imaging the extracellular space between glass and adjacent plasma membrane using rhodamine-dextran, which reveals close adhesions by dextran exclusion (Gingell et al., 1985); and (2) imaging plasma-membrane-associated MARCKS-GFP (Groves et al., 2008; Toomre and Manstein, 2001).

Fig. 6A (left) shows exclusion of rhodamine-dextran along the edge of a WM-1617 cell transfected with GFP alone. The dark areas indicate narrowed cell-substratum contacts. GFP fluorescence was spread throughout the cell, and, as shown in the merged image, extended beyond the close adhesions along the cell edge. This generated a yellow border (indicated by arrows), about 0.8±0.1 μm wide, because of the enhanced overlap of GFP and rhodamine-dextran (the fine adherent filopodia seen by dextran exclusion were not filled with GFP and, thus, not visible with this cytosolic marker). Fig. 6B illustrates this labeling pattern schematically. When MARCKS-GFP was expressed, the cell edge was decorated with an increased number of filopodia, which excluded dextran (and, thus, were adherent) and emitted strong MARCKS-GFP fluorescence. The merged image shows precise overlap between the two images, indicating that MARCKS colocalized with the close adhesions along the cell edge (see also Fig. 6A,B). These results also suggested that the leading edge forms a small ‘overhang’ that is not attached to the substratum and devoid of membrane-associated MARCKS (Fig. 6C, profile).

IRM images revealed further differences. GFP-only cells exhibited the close contact areas, including focal adhesions (black arrows), that we had observed in nontransfected cells. MARCKS-GFP cells, however, had larger close-contact areas suggesting increased attachment. This was assessed by measuring total adherent cell area (Fig. 5D). Quantitative analysis demonstrated a highly significant (P≤0.002), almost twofold increase in cell area for the MARCKS-GFP cells. To determine whether enhanced cell spreading was related to an increase in focal adhesions, we counted these adhesions in IRM images. The mean number of focal adhesions in GFP-only cells (18.4±1.5 per cell; mean ± s.e.m., n=14) was essentially identical to that in MARCKS-GFP-expressing cells (18.9±1.7 per cell, n=14). Furthermore, focal adhesions in control and MARCKS-GFP transfectants seemed to have the same size and configuration. In other words, MARCKS-GFP expression did not affect focal adhesions.

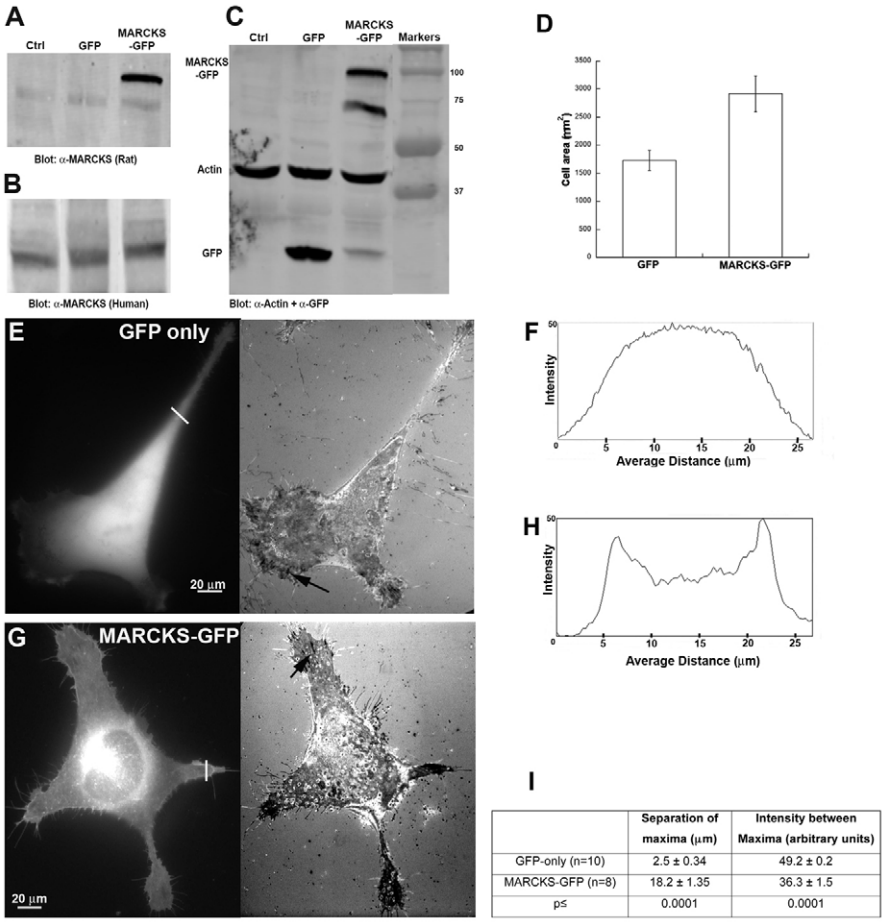

	Separation of maxima (μm)	Intensity between Maxima (arbitrary units)
GFP-only (n=10)	2.5 ± 0.34	49.2 ± 0.2
MARCKS-GFP (n=8)	18.2 ± 1.35	36.3 ± 1.5
p≤	0.0001	0.0001

Fig. 5. Effect of MARCKS-GFP overexpression on cell adhesion and size. Cells were transfected with either rat MARCKS-GFP plasmid or GFP plasmid, or they were mock-transfected for control (Ctrl). After 24 hours, cells were lysed and equal amounts of protein (120 μg/lane) loaded on SDS-polyacrylamide gels. Western blots were probed with antibodies to rat MARCKS (A), human MARCKS (B), or GFP and actin (C). In the MARCKS-GFP lane in C, the GFP immunoreactive bands at about 75 and 27 kDa are probably breakdown products. (D) Total adherent areas of cells transfected with GFP only versus MARCKS-GFP ($P \leq 0.002$). Fluorescent and IRM micrographs of cells transfected with GFP alone (E) and with MARCKS-GFP (G). Black arrows indicate focal adhesions. (F,H) Fluorescence intensity profiles (arbitrary units) of representative GFP and MARCKS-GFP cells, respectively (locations of scans are shown as white lines in E and G). (I) Quantitative analysis of intensity scans. Means ± s.e.m. (n=10 for GFP alone; n=8 for MARCKS-GFP), and statistical significance (Student's t-test) are shown.

To evaluate whether overexpressed MARCKS was phosphorylated in response to TPA treatment, untransfected cells (control), mock-transfected cells (mock), GFP-only cells, and MARCKS-GFP-transfected cells were treated with 1 μM TPA for 10 minutes at 37°C, lysed, and processed for western blot. As a loading control for MARCKS protein, we used actin (left). Human MARCKS served as control for the amount of endogenous MARCKS protein in the phosphorylated sample (right). Fig. 7A documents expression of MARCKS-GFP in MARCKS- versus control-transfected cells. The blot on the right, probed with antibody to rat MARCKS-*P*, shows that treatment with TPA increased (about twofold) the amount of MARCKS-*P*-GFP (prominent upper band). Weak crossreactivity of the antibodies also revealed a faint lower band of endogenous (human) MARCKS (left). A corresponding band of human MARCKS-*P* (right) was barely visible in the TPA-stimulated MARCKS-GFP lane. Precise quantitative comparison between the MARCKS and MARCKS-*P* blots was impossible because the antibody affinities were unknown. Assuming similar affinities, scans would suggest that less than 20% of MARCKS-GFP was phosphorylated.

The effects of MARCKS gain-of-function were explored further in experiments using PKC stimulation to trigger dissociation of

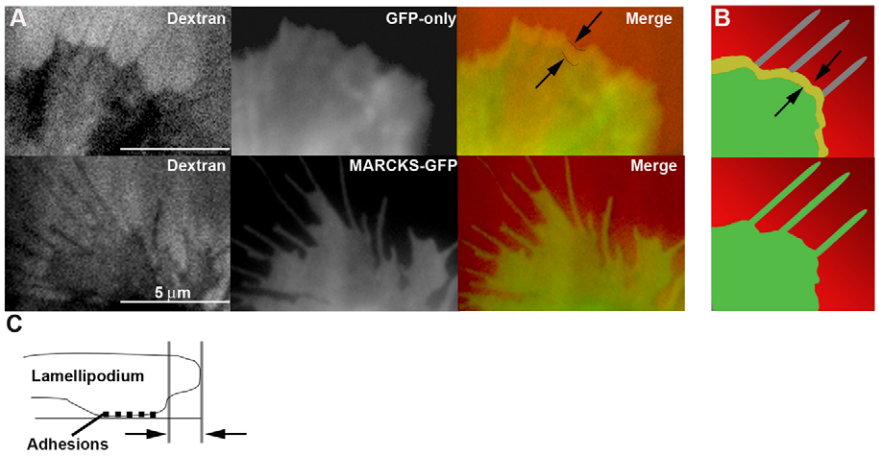

Fig. 6. Relative distribution of close adhesions and MARCKS-GFP. (A) TIRF images of rhodamine-dextran and either GFP alone (top) or MARCKS-GFP (bottom) in WM-1617 cells. In the dextran exclusion images the dark areas indicate close cell-substratum contact. Note that filopodia are labeled with MARCKS-GFP (bottom) but not with GFP alone (top). (B,C) Cartoons explaining results in the merged images. B shows schematically the distribution of GFP relative to close adhesions as revealed by dextran exclusion (top). The resulting overhang (between arrows) is shown in cross section in C. By contrast, MARCKS-GFP fluorescence overlaps completely with dextran exclusion (B, bottom).

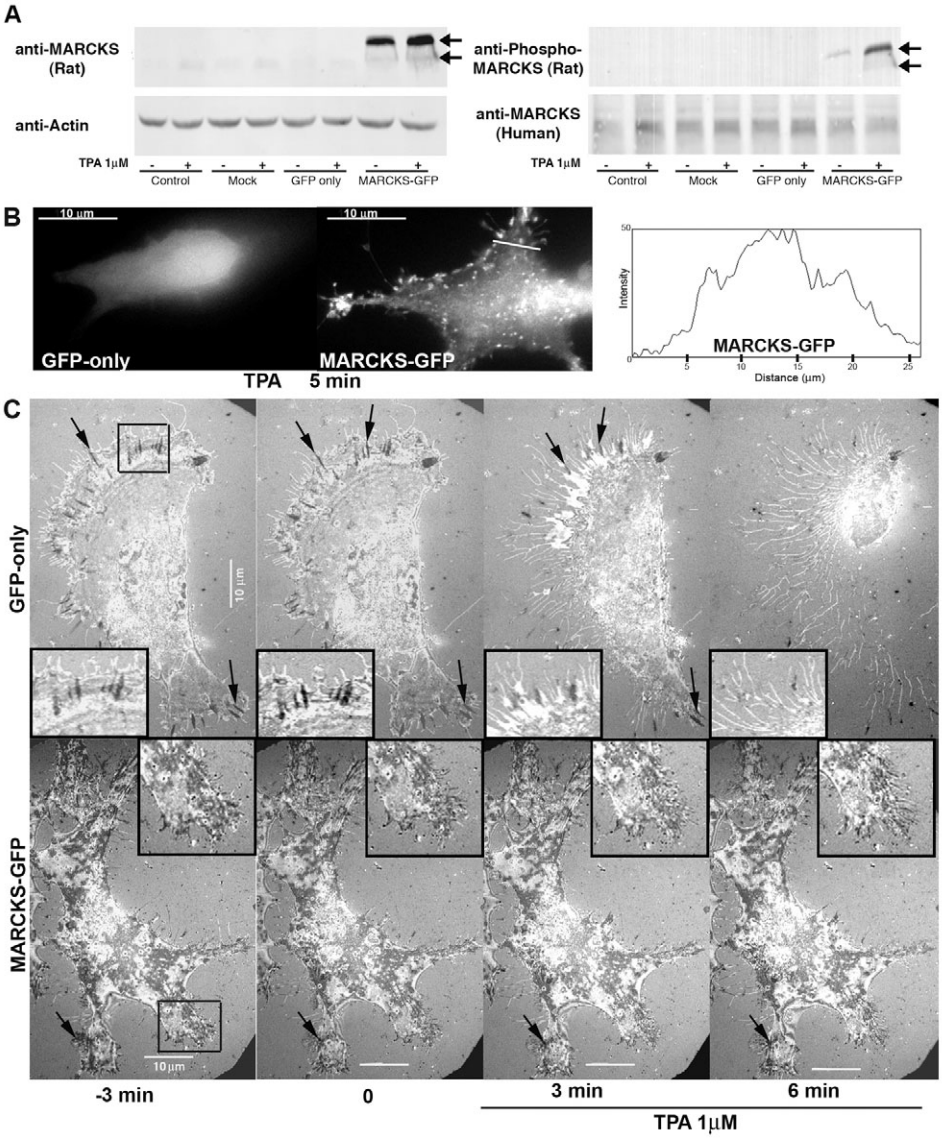

Fig. 7. Effect of MARCKS overexpression on TPA-stimulated cell detachment (WM-1617 melanoma). (A) Nontransfected cells (Ctrl, mock) and cells transfected with either GFP or MARCKS-GFP were treated with 1 μM TPA. Total cell lysates (70 μg protein per lane) were subjected to immunoblot analysis using anti-MARCKS (rat), anti-MARCKS-*P* (rat) and, as loading controls, anti-actin and anti-MARCKS (human) antibodies. Arrows indicate MARCKS-GFP (upper arrow) and a weak lower band of endogenous human MARCKS (lower arrow, especially on left). (B) Cells transfected with GFP-only or MARCKS-GFP were treated with 1 μM TPA for 5 minutes. Fluorescence micrographs were taken and intensity profiles analyzed. White line indicates the position of the scan use to generate the profile (right). (C) IRM images, taken at 3-minute intervals (0 minutes, onset of TPA treatment), of a GFP-transfected cell (top row) and of a MARCKS-GFP-transfected cell (bottom row) challenged with 1 μM TPA. Magnifications of the adhesions are shown in insets. Black arrows indicate focal adhesions.

adhesion. Because of its strong activation of the kinase, we used TPA for these experiments. First, we examined the effects of TPA on MARCKS-GFP distribution. To capture GFP distribution, we fixed cultures after 5 minutes of TPA exposure by rapid addition of formaldehyde fixative, before image acquisition. In contrast to control cells, which retracted rapidly (Fig. 7B, left) MARCKS-GFP cells remained spread out and exhibited small fluorescent patches along the plasma membrane and the cell edge (Fig. 7B, right). However, between the patches, edge labeling had disappeared, as indicated by intensity scan (Fig. 7B, far right; see Fig. 5E-H for comparison). Thus, strong PKC activation moved some MARCKS-GFP (except for that contained in membrane patches) away from the plasma membrane. We monitored the effects of TPA on cell contact by IRM. Before bath application of 1 μM TPA, GFP-only cells exhibited the familiar image of close adhesions near the cell margin, interspersed with focal adhesions (–3 and 0 minutes, top panels in Fig. 7C; see also inserts). By 3 minutes after TPA application, cellular retraction was evident, and close adhesions, except for some of the focal adhesions, had given way to wider, IRM-bright contacts (Izzard and Lochner, 1976). By 6 minutes, most of the cell contact area had disappeared, leaving behind only filamentous elements attached via wider contacts (n=6). The same experiment performed with MARCKS-GFP cells (bottom panels in Fig. 7C; n=6) revealed large expanses of close contacts before TPA application, as described above (Fig. 5G). These close contacts remained essentially unchanged 3 and even 6 minutes after TPA application. In addition, total cell area did not obviously decrease. It follows that MARCKS gain-of-function rendered WM-1617 cells refractory to TPA-induced detachment, for at least 6 minutes.

Immunolocalization of adhesion markers

The results described above suggested a unique role of MARCKS in cell adhesion. Therefore, we studied its distribution, relative to integrin α3 and the classic focal-adhesion markers, vinculin and paxillin, in cells plated on laminin. Immunofluorescence micrographs were acquired as *z*-stack images and digitally deconvolved to extract images of the adherent plasma membrane. WM-1617 cells are shown in Fig. 8A-C. Double-labeling of MARCKS and integrin α3 showed a spotted distribution of both labels with substantial colocalization along the distal edges of spread-out cellular areas (Fig. 8A). This overlap was analyzed quantitatively in deconvolved images of the leading edge of 10 cells

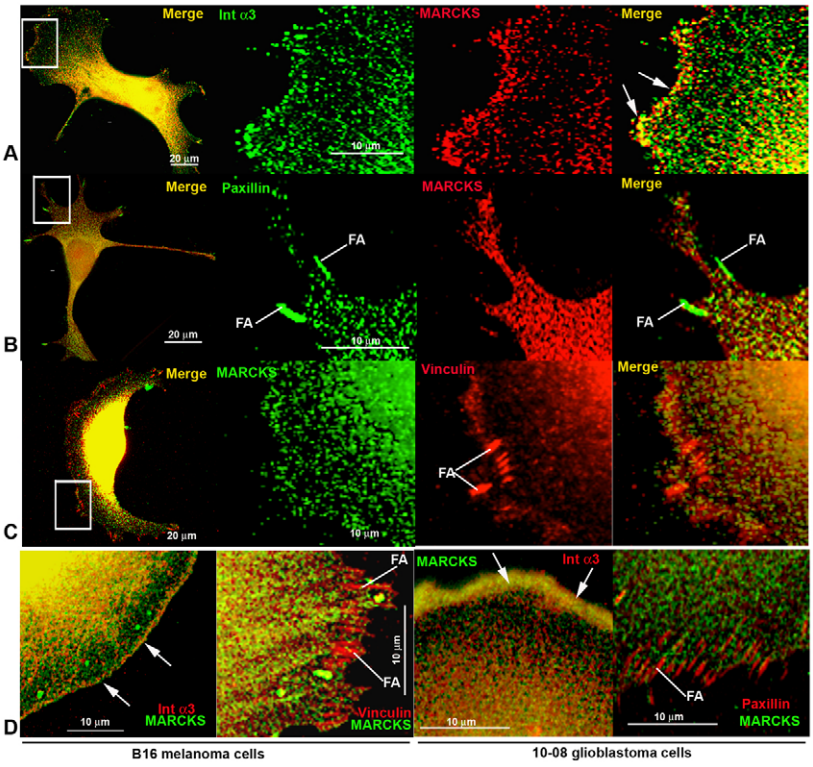

Fig. 8. Localization of MARCKS, α3-integrin, paxillin, and vinculin in three different tumor cell lines on laminin. All images are digitally deconvolved fluorescence micrographs of the attached plasma membrane. For A-C, the first image in each row shows the merged image (overlap in yellow) of the complete cell (WM-1617); subsequent images show the specified region at higher power. (A) Anti-α3-integrin and anti-MARCKS. Arrows indicate a region of overlap along the cell edge. (B) Anti-paxillin and anti-MARCKS. Note that focal adhesions (FA) are devoid of MARCKS. (C) Anti-MARCKS and anti-vinculin. There is essentially no overlap between MARCKS and vinculin in the cell periphery. (D) Fluorescence micrographs of B16 melanoma cells (left) labeled with anti-α3-integrin, anti-MARCKS and anti-vinculin. 10-08 glioblastoma cells immunolabeled with anti-MARCKS, anti-integrin α3 and anti-paxillin are shown on the left. Arrows indicate a ribbon of overlap of MARCKS and α3 integrin. FA, focal adhesions.

(≥30 μm^2 of contiguous area each). Two different, unbiased thresholding approaches were used to calculate overlap coefficients for either the combined channels or for each channel separately. Manders' coefficient R ranges from 0 to 1, indicating no or complete colocalization, respectively. Values for R are influenced by the channel ratio (green for α3 integrin, red for MARCKS) and should be near 1. In our analysis, the average channel ratio was 1.36±0.38 (± s.e.m.), and Manders' coefficient *R* was 0.78±0.04. The more stringent threshold overlap coefficients, R_T (calculated separately for each channel), were 0.57±0.07 for integrin α3 and 0.45±0.07 for MARCKS. This meant that 57% of integrin-α3-positive pixels colocalized with MARCKS-positive pixels, and that 45% of MARCKS-positive pixels overlapped with integrin-α3-positive pixels (all above background). Thus, both analyses indicated substantial colocalization.

The fine punctate distribution of the label was at variance with that of MARCKS-GFP in live cells (Fig. 5) and might have been caused by fixation and/or antibody labeling. This punctate pattern does not affect the localization data, but its significance is unclear. Focal adhesions were not positive for integrin α3 and could not be discerned in these samples. By contrast, labeling with antibodies to paxillin or vinculin clearly revealed focal adhesions, but there was no colocalization with MARCKS (Fig. 8B,C). In thinly spread areas, paxillin and vinculin label was spotted outside of focal adhesions, with some MARCKS colocalization for paxillin, but very little for vinculin.

If this labeling pattern was characteristic of dynamic adhesions, it had to be consistent for different cell types. Therefore, we examined the distribution of MARCKS, α3 integrin, paxillin and vinculin in B16 melanoma and 10-08 glioblastoma cells. MARCKS was absent from focal adhesions, and a ribbon of colocalization of MARCKS and integrin α3 was also evident along the lamellipodial edge in these cells (Fig. 8D). In fact, the adhesive ribbons were more prominent than those in WM-1617 cells. These results show that the ribbon-like adhesive structure observed in Fig. 1 correlates with immuno-colocalization of α3 integrin and MARCKS in several cell types.

Discussion

IRM imaging of melanoma cells revealed the presence of two prominent types of close contact, focal adhesions and the more transient dynamic adhesions. The latter generally cover larger areas and often are located along the edges of the thinned-out cell periphery. So-called focal contacts, which are small, punctate close adhesions, also may have been formed by the melanoma cells but were not analyzed. Our results provide insights into the microscopic and biochemical properties that characterize dynamic adhesions and into the mechanisms that regulate their detachment. Of particular interest was the role of MARCKS in dynamic adhesions.

PKC activation and cell detachment

It has been reported that the arachidonic acid metabolite 12(S)-HETE promotes metastatic behavior of tumor cells (Szekeres et al., 2002; Tang et al., 1995). Exogenous application of the eicosanoid causes 'non-focal' close adhesions, i.e. dynamic adhesions, to detach rapidly, whereas focal adhesions change slowly. This differential sensitivity to 12(S)-HETE functionally distinguishes focal adhesions from dynamic adhesions.

PKC is known to participate in cell motility and adhesion (Brandt et al., 2002; Disatnik et al., 2004; Woods and Couchman, 1992). Protein phosphorylation assays and IRM demonstrated that 12(S)-HETE, similarly to TPA, activated PKC in melanoma cells, and that this effect was blocked by Bis, which selectively inhibits the isoforms PKCα, PKCβI, PKCβII, and PKCε (Toullec et al., 1991). Our results demonstrate that, in WM-1617 cells, PKCε is the much more prominent isoform than PKCα, and that PKCβ and PKCγ are essentially absent. This is consistent with the reported reduction or

absence of these isoforms in different melanoma lines (Becker et al., 1990; Gilhooly et al., 2001; Linnenbach et al., 1988; Oka and Kikkawa, 2005; Oka et al., 1996). Based on our previous results (Mikule et al., 2003) and the data on PKC isoform abundance shown here, the effect of 12(S)-HETE is likely to be mediated by PKCε.

MARCKS is a major PKC substrate that has been implicated in cellular migration and adhesion (Aderem, 1992; Blackshear, 1993; Disatnik et al., 2004). The data reported here identify MARCKS as the predominant PKC substrate. They demonstrate that nonphosphorylated MARCKS is membrane associated, and that phosphorylation triggers its translocation into the cytosol. MARCKS needs to move, in PKC-dependent manner, between membrane and cytosol to promote adhesion (Gatlin et al., 2006; Kim et al., 1994; McLaughlin and Aderem, 1995; Rombouts et al., 2008). Our microscopic and biochemical observations suggest that eicosanoid-induced detachment of dynamic adhesions is paralleled by PKC activation, MARCKS phosphorylation and dissociation of MARCKS-*P* from the plasma membrane.

Role of MARCKS in cell adhesion

Cell adhesion and motility are initiated by the binding of integrins to their ligands in the extracellular matrix (Hynes, 1992). Integrin activation is accompanied by the formation of adhesion complexes and the reorganization of the actin cytoskeleton (Disatnik et al., 2004; Woods and Couchman, 1992). In WM-1617 and B16 melanoma cells, as well as in 10-08 glioblastoma cells, deconvolved fluorescence micrographs of the adherent plasma membrane show enrichment of MARCKS immunoreactivity in the periphery of well-spread processes, where close adhesions are often found (compare Fig. 1A and Fig. 8A). These are the same regions where integrin α3 immunofluorescence is concentrated and, indeed, colocalized with MARCKS. This colocalization in dynamic adhesions suggests that MARCKS is involved in integrin-mediated cell attachment.

It is technically not possible at present to image close adhesions (by IRM) and immunoreactivity of their components simultaneously, because dynamic adhesions change too rapidly relative to the effect of aldehyde fixation, and aldehyde fixation induces extensive IRM artifacts. However, our TIRF images of dextran exclusion and MARCKS-GFP indicate that MARCKS localizes to plasma membrane domains involved in dynamic adhesion.

The association of MARCKS with dynamic adhesions suggests that MARCKS gain-of-function should increase adhesive area, but not the number or size of focal adhesions. We demonstrate that MARCKS-GFP is associated largely with the plasma membrane of WM-1617 cells, and that increased MARCKS expression broadens total cell area to almost twice that observed in GFP-only controls. However, focal adhesions do not increase in number and apparently not in size. These results were not an artifact of the fusion protein because MARCKS-GFP cycles normally between plasma membrane and cytosol (Ohmori et al., 2000; Sawano et al., 2002). Adhesion of MARCKS-GFP-transfected cells was also more resistant to PKC stimulation. MARCKS-GFP cells showed no signs of detachment upon application of TPA at a time when GFP-only controls had detached almost completely. This resistance to PKC activation suggests that overexpressed MARCKS stabilizes dynamic adhesions, namely integrin attachment to the substratum, and that PKC activity might be insufficient to phosphorylate and cytosolically translocate the amounts of MARCKS necessary for triggering detachment. Indeed, although MARCKS-GFP was phosphorylated in our experiments, the amount of phosphoprotein relative to total protein appeared to be small.

Our results suggest that MARCKS stabilizes dynamic adhesions. This conclusion seems to contradict the observations that expression of constitutively membrane-associated mutant MARCKS inhibited initial stages of cell attachment (Myat et al., 1997; Spizz and Blackshear, 2001; Swierczynski and Blackshear, 1995). However, studies on well-attached, widely spread cells and nerve growth cones suggested that MARCKS enhanced cell to matrix adhesion (Gatlin et al., 2006; Iioka et al., 2004; Manenti et al., 1997), as in our melanoma experiments. Thus, MARCKS seems to both inhibit cell spreading and stabilize adhesion of attached cells. This paradox remains to be explained. MARCKS might maintain integrins in their high-affinity state, thus stabilizing adhesions. It also might limit their lateral mobility, which is necessary for de-novo adhesion formation, and thus inhibit attachment (Li et al., 1996).

Focal adhesions versus dynamic adhesions

Adhesions have been classified based on their composition and morphology (Lock et al., 2008; Webb et al., 2003; Webb et al., 2002; Worth and Parsons, 2008). Table 1 shows recent classifications and characteristics. However, the use of the term ‘focal’ for several of the adhesions causes confusion, and the distinctions among the categories are not always clear.

Comparison of focal adhesions and dynamic adhesions reveals major structural and functional differences. Focal adhesions are anchor sites for actin cables that inhibit cell migration rather than supporting it (Broussard et al., 2008; Lock et al., 2008; Webb et al., 2002). They have a characteristic, elongated configuration and resist extraction by Triton X-100. They contain integrins, in particular αvβ3 integrin, which binds fibronectin and vitronectin, and cytoplasmically associated proteins such as paxillin and, especially, vinculin (Webb et al., 2003; Webb et al., 2002). By contrast, dynamic adhesions are irregularly shaped and larger, and typically located along the edges of widely spread cell processes. Physiologically, focal adhesions that form near the front of migrating cells remain fixed to the substrate as the cell moves. This stationary status helps the cell to resist the contraction that allows the cell body to move (Sastry and Burridge, 2000). In studies of fibroblasts, focal adhesions could move relative to the substrate (Smilenov et al., 1999). However, these cells were not migrating, making it difficult to compare the results with those in highly motile cells. Overall, focal adhesions do not support locomotion, are sparse or absent from migratory cells, and are most prominent in stationary cells (Burridge and Chrzanowska-Wodnicka, 1996; Burridge et al., 1988; Sastry and Burridge, 2000).

In contrast to focal adhesions, dynamic adhesions change rapidly, and they detach within minutes of exposure to the PKCε-activating eicosanoid, 12(S)-HETE. In addition to eicosanoid sensitivity, our results indicate further molecular differences between focal and dynamic adhesions, such as the solubility of dynamic adhesions in Triton X-100. (A.E.-B. and K.H.P., unpublished).

Dynamic adhesions are most similar to focal complexes and nascent adhesions (Table 1). Focal complexes have been described as small, punctate adhesions near the leading edge, beneath the actin meshwork (Kaverina et al., 2002; Nobes and Hall, 1995; Webb et al., 2003). They are induced by Rac1 and Cdc42 activation, contain β1 integrin and can mature into focal adhesions (Webb et al., 2003; Webb et al., 2002). Nascent adhesions are very similar to focal complexes and form near the leading edge of migrating cells (Choi et al., 2008). They contain paxillin and vinculin and can mature to focal adhesions in a myosin-II-dependent manner. Even though dynamic adhesions resemble focal complexes and nascent

Table 1. Classification and characteristics of adhesion complexes

Adhesion type	Characteristics	References
Focal adhesions	Large oval-shaped structures; include paxillin, vinculin, αvβ3 integrin and tyrosine-phosphorylated proteins; inhibit migration	(Burridge and Chrzanowska-Wodnicka, 1996; Katz et al., 2000; Lock et al., 2008; Webb et al., 2003; Zamir and Geiger, 2001)
Fibrillar adhesions	Elongated, central structures; contain tensin and α5β1 integrin; low levels of paxillin, vinculin and tyrosine-phosphorylated proteins	(Lock et al., 2008; Pankov et al., 2000; Webb et al., 2003)
Focal complexes	Small adhesions near leading edge; induced by Rac activation; can mature into larger, more organized focal adhesions; postulated to drive migration	(Beningo et al., 2001; Lee and Jacobson, 1997; Lock et al., 2008; Nobes and Hall, 1995; Rottner et al., 1999; Webb et al., 2003)
Podosomes	Invasive ring structures composed of adhesion machinery and filamentous actin	(Lock et al., 2008; Webb et al., 2003)
Focal points	'Nascent adhesions' formed in the cellular periphery that link to an F-actin meshwork	(Lock et al., 2008)
Nascent adhesions	Contain vinculin; often maturation to focal adhesions in a myosin II dependent manner	(Choi et al., 2008)
Dynamic adhesions	No vinculin; no conversion into focal adhesion; contain MARCKS and α3β1 integrin	This report

adhesions, they differ significantly in that they do not contain vinculin and do not mature to focal adhesions. They maintain their position at, and advance with, the leading edge of the cell, and do not seem to spawn other adhesive structures. This suggests that these dynamic structures are subject to the highly active turnover taking place at the leading edge of the cell.

Lee and Jacobson described a different type of adhesion in fish keratocytes that they described as close contacts containing β1 integrin, talin, vinculin, α-actinin, paxillin and FAK (Lee and Jacobson, 1997). They also reported that close contacts and focal adhesions were interconvertible because the continued accumulation of additional molecules in close contacts could originate focal adhesions. Thus, the keratocyte close contacts closely resemble focal complexes and nascent adhesions. Nevertheless, keratocyte close contacts, like dynamic adhesions, form an adhesive rim at the leading edge, which is enriched in β1 integrin. Based on these observations, we suggest that what these authors reported as close contacts (Lee and Jacobson, 1997) are actually focal complexes and/or nascent adhesions, and that the outer rim of these close contacts is what we define here as dynamic adhesions.

The fact that diverse but highly motile cell types, such as melanoma cells, glioma cells and growing neurons [growth cones (Gatlin et al., 2006)] contain dynamic adhesions suggests that these adhesions are common features of rapid cell movement. MARCKS emerges as a likely specific molecular 'marker' of dynamic adhesions, because of its complete absence from focal adhesions and colocalization with integrin α3β1 at the leading edge of the cell. Overall, molecular differences between dynamic and other adhesive structures are becoming evident.

Conclusions

Our results describe rapidly changing, ribbon-like close adhesions, named 'dynamic adhesions' in highly motile tumor cells. Dynamic adhesions are characterized by MARCKS colocalized with integrin α3, but do not contain the focal adhesion marker, vinculin. Also, they do not mature into focal adhesions, which distinguishes them from focal complexes and nascent adhesions. Dynamic adhesions, unlike focal adhesions, are highly sensitive to PKCε activation, for example, by the eicosanoid 12(S)-HETE. Eicosanoid-induced cell detachment seems to be triggered by MARCKS phosphorylation and dissociation from the plasma membrane. Thus, MARCKS is a stabilizer of dynamic adhesions, regulated via PKCε-mediated phosphorylation.

Materials and Methods

Materials

Reagents were obtained from the following suppliers: 12(S)-HETE from Biomol; tetradecanoyl phorbol acetate (TPA) and bisindolylmaleimide I (Bis) from Sigma (St Louis, MO); fetal bovine serum (FBS) from Atlanta Biologicals (Lawrenceville, GA). Antibodies: anti-MARCKS for western blot from Upstate-Millipore (Billerica, MA) and Santa Cruz Biotechnology (Santa Cruz, CA); anti-MARCKS for immunofluorescence from Proteintech Group (Chicaco, IL); anti-phosphoMARCKS from Cell Signalling Technology (Danvers, MA); anti-α3-integrin from Developmental Studies Hybridoma Bank (University of Iowa, IA); anti-GFP from Abcam (Cambridge, MA); anti-actin and anti-vinculin from Sigma; anti-paxillin from Biosource (Invitrogen, Carlsbad, CA); PKC isoform-specific antibodies from BD Biosciences (Franklin Lakes, NJ); anti-lactate dehydrogenase (LDH) from Rockland (Gilbertsville, PA); horseradish peroxidase (HRP)-conjugated antibody from Vector (Burlingame, CA); all other secondary antibodies from Molecular Probes (Eugene, OR). Additional chemicals, unless stated otherwise, were from Sigma and were of the highest quality available.

Cell culture

WM-1617 melanoma cells, a generous gift from David A. Norris at the Department of Dermatology (University of Colorado School of Medicine, Aurora, CO), were cultured in RPMI 1640 medium supplemented with 10% heat-inactivated fetal bovine serum (FBS), 2 mM L-glutamine and 100 U/ml penicillin-streptomycin. B16 (F10) mouse melanoma cells were from ATCC (Manassas, VA) and cultured in DMEM-GlutaMAX supplemented with 4.5 g/l glucose, 110 mg/l sodium pyruvate, 10% heat-inactivated FBS. 10-08 glioblastoma cells (generous gift from Carol Kruse, Sidney Kimmel Cancer Center, San Diego, CA) were cultured in DMEM supplemented with 10% heat-inactivated FBS and 2 mM L-glutamine. Cells were grown in a humidified atmosphere containing 5% CO_2.

Cell transfection

A plasmid (pEGFP-N1; Clontech, Mountain View, CA) containing wild-type MARCKS fused at its C-terminus with GFP was generated previously (Gatlin et al., 2006). The same plasmid without the MARCKS insert was used as a control. Cells plated on laminin were transfected at 60-80% confluence using FuGene 6 (Roche Diagnostics, Indianapolis IN) and 2 μg plasmid DNA, according to the manufacturer's instructions. Cells were incubated for 24 hours before microscopic or biochemical analysis.

Microscopy

Images were acquired with a Zeiss Axiovert 200M microscope with Zeiss optics, Cooke Sensicam digital camera, and Metamorph software (Molecular Devices, Sunnyvale, CA). Cells plated for 24 hours on laminin-coated coverslips were placed in an open chamber with medium, layered over with inert mineral oil (embryo tested, sterile filtered) to avoid evaporation and maintain pH, and examined under convective heating at 37°C. For certain experiments, effectors were introduced into the cultures

by repetitive pulse application with a micropipette (inner tip diameter 1-2 μm) and Picospritzer system (6 p.s.i.; General Valve, Fairfield, NJ) to create a gradient (Gatlin et al., 2006; Lohof et al., 1992). The micropipette was filled with 10^{-8} M 12(S)-HETE and its tip placed 100 μm away from the cell. Repetitive pulse ejection of the reagent generated a stable, shallow gradient decreasing to about 10^{-10} M near the cell (Lohof et al., 1992). Alternatively, effectors were diluted into the medium.

Adhesions were analyzed by IRM, which generates images based on the distance between the plasma membrane and the growth substratum (Izzard and Lochner, 1976). Images were captured with a digital camera at different times before and after application of reagents. Close adhesions were quantified using area measurement (ImageJ). To determine areas of cell-substratum contact we examined cells in phase contrast.

To establish edge labeling of cells quantitatively, we analyzed intensity scans across cellular processes. Because of the considerable differences in fluorescence intensities, scans were normalized by setting intensity maxima to 50 arbitrary units. Intensities were plotted against the distance between half-maximal intensities (the 'flanks' of cell process scans). Next, we determined for each profile the distance between the two highest peaks and the intensities of the scans in the middle between the two maxima.

For TIRF microscopy, cells plated on laminin-coated glass bottom dishes were examined with a Zeiss Alpha Plan-Apo ×100 objective (NA=1.46), in combination with a TIRF illuminator coupled to an argon ion laser and filter cubes optimized for GFP, Alexa Fluor 488 and rhodamine (Chroma Technology). For dextran-exclusion experiments, the medium contained 100 mg/ml of rhodamine-dextran (M_r 10,000) and cells were incubated for 2 hours before analysis.

Fixation and immunofluorescence

Cells were fixed using slow infusion of 4% (wt/vol.) formaldehyde in 0.1 M phosphate buffer, pH 7.4, with 120 mM glucose and 0.4 mM $CaCl_2$ (Pfenninger and Maylie-Pfenninger, 1981). Cultures were rinsed with phosphate-buffered saline (PBS) containing 1 mM glycine, permeabilized with blocking buffer [PBS, 3% (wt/vol.) bovine serum albumin] plus 1% (vol./vol.) Brij 98 detergent for 2 minutes at room temperature, and placed in blocking buffer for 1 hour at room temperature. Cultures were incubated with the primary antibodies for 1 hour at room temperature and washed three times with blocking buffer. This process was repeated with the appropriately tagged secondary antibodies [Alexa Fluor 488 (green) and Alexa Fluor 594 (red)]. Coverslips were mounted on slides with SlowFade Gold antifade reagent (Invitrogen-Molecular Probes, Eugene, OR). Where indicated, we digitally deconvolved image stacks to reveal the optical section that included the attached plasma membrane and adhesion-associated proteins.

Colocalization analysis

Digitally deconvolved (nearest neighbor) images of WM-1617 cells were analyzed using ImageJ software. To exclude background in an unbiased manner, we proceeded in two ways: (1) We thresholded all images by limiting the eight-bit display range to 10-255 and calculated Manders' coefficient (R) by using the appropriate plug-in. (2) We performed automatic threshold calculation in conjunction with overlap analysis (R_T coefficient) using the 'Colocalization Threshold' plug-in [(Costes et al., 2004); ImageJ Web site, Wright Cell Imaging Facility, Toronto Western Research Institute www.uhnresearch.ca/wcif]. In both cases, zero/zero pixels were excluded from the analysis.

Kinase assays

In whole-cell assays we analyzed PKC activity using endogenous substrate, in the absence of Ca^{2+}. The protocol was essentially as described by Katz et al. (Katz et al., 1985). Briefly, 3×10^6 cells were plated in culture dishes for 2 hours, washed with ice-cold Hank's balanced salt solution (HBSS) and collected in 'kinase buffer' (20 mM HEPES pH 7.0, 10 mM $MgCl_2$, 1 mM EGTA, 200 mM NaF, 100 mM Na_3VO_4, and protease inhibitor cocktail). Effectors were added for 10 minutes at 4°C (10^{-8} M HETE, 1 μM TPA and/or 10 nM Bis) and cells permeabilized with 0.01% saponin to allow radiolabeled exogenous ATP to enter. Cells were warmed to 30°C and reactions initiated with 50 μM ATP plus 3 μCi [γ-^{32}P]ATP. After 1 minute, the reaction was stopped by addition of the PKC inhibitor, calphostin C (Sigma). The permeabilized cells were pelleted and the supernatant collected as cytosol fraction. Pellets were rinsed with PBS and extracted with 0.5% Triton X-100 in PBS for 30 minutes on ice. Supernatant was collected as the Triton-soluble fraction. The pellet was rinsed and recovered with RIPA buffer containing 1 mM EDTA as the Triton-X-100-insoluble fraction. Samples were chloroform-methanol precipitated, solubilized in SDS and loaded on SDS-polyacrylamide gels for electrophoresis. Phospho-polypeptides were detected by storage phosphor imaging (Typhoon 9400 multi-mode imager; GE Healthcare, Piscataway, NJ).

Kinase assay and MARCKS immunoprecipitation

Anti-MARCKS antibody (5 μg) was added to 500 μg protein of the cytosol fraction derived from the kinase assay just described and incubated at 4°C for 2 hours. 50 μl protein A/G-coupled agarose beads (Calbiochem-EMD, San Diego, CA) was added and incubated for 1 hour. Beads were spun out and the supernatant collected. The beads were washed three times with cold PBS, resuspended in Laemmli sample buffer, and proteins resolved by gel electrophoresis. Phospho-polypeptides were detected by storage phosphor imaging.

Fractionation analysis of MARCKS

Procedures were modified from Disatnik et al. (Disatnik et al., 2002). 3×10^6 cells were plated on each culture dish and incubated at 37°C for 2 hours. Effectors were added for 10 minutes at 37°C. Subsequently cells were washed with cold HBSS and scraped off in cold homogenization buffer (50 mM Tris-HCl, 1 mM EDTA, 1 mM EGTA, 200 mM NaF, 100 mM Na_3VO_4, and protease inhibitor). This suspension was passed through a 22-gauge needle. After spinning at 100,000 ***g*** for 30 minutes at 4°C, the cytosolic fraction was collected and the membrane pellet solubilized in RIPA buffer. Both samples were mixed with Laemmli buffer and resolved on 7.5% SDS-polyacrylamide gels. MARCKS levels were determined by western immunoblot and fluorescence scanner analysis.

Gel electrophoresis and western blot analysis

Samples were resolved by SDS-polyacrylamide gel electrophoresis and electro-transferred onto polyvinylidene fluoride (PVDF) membranes. Blots were blocked with 5% non-fat milk and 0.1% Tween-20 in TBS for at least 1 hour and then incubated with primary antibody for 1 hour at room temperature. After three rinses with TBS-Tween-20, blots were incubated with secondary antibody (HRP or fluorophore conjugated) for 1 hour and rinsed. Bound antibody was detected by enhanced chemiluminescence on film or by fluorescence imaging.

We thank our colleague Rytis Prekeris for the pEGFP-N1 plasmid and Agne Taraseviciute for help with gradient images. The α3 integrin antibody (Ralph 3.1), developed by L. Reichardt, was obtained from the Developmental Studies Hybridoma Bank developed under the auspices of the NICHD and maintained by The University of Iowa, Department of Biological Science, Iowa City, IA 52242. This work was supported by NIH grant R01 NS41029. Deposited in PMC for release after 12 months.

References

Aderem, A. (1992). The MARCKS brothers: a family of protein kinase C substrates. *Cell* **71**, 713-716.

Aderem, A. (1995). The MARCKS family of protein kinase-C substrates. *Biochem. Soc. Trans.* **23**, 587-591.

Becker, D., Beebe, S. J. and Herlyn, M. (1990). Differential expression of protein kinase C and cAMP-dependent protein kinase in normal human melanocytes and malignant melanomas. *Oncogene* **5**, 1133-1139.

Beningo, K. A., Dembo, M., Kaverina, I., Small, J. V. and Wang, Y. L. (2001). Nascent focal adhesions are responsible for the generation of strong propulsive forces in migrating fibroblasts. *J. Cell Biol.* **153**, 881-888.

Blackshear, P. J. (1993). The MARCKS family of cellular protein kinase C substrates. *J. Biol. Chem.* **268**, 1501-1504.

Brandt, D., Gimona, M., Hillmann, M., Haller, H. and Mischak, H. (2002). Protein kinase C induces actin reorganization via a Src- and Rho-dependent pathway. *J. Biol. Chem.* **277**, 20903-20910.

Broussard, J. A., Webb, D. J. and Kaverina, I. (2008). Asymmetric focal adhesion disassembly in motile cells. *Curr. Opin. Cell Biol.* **20**, 85-90.

Burridge, K., Fath, K., Kelly, T., Nuckolls, G. and Turner, C. (1988). Focal adhesions: transmembrane junctions between the extracellular matrix and the cytoskeleton. *Annu. Rev. Cell Biol.* **4**, 487-525.

Burridge, K. and Chrzanowska-Wodnicka, M. (1996). Focal adhesions, contractility, and signaling. *Annu. Rev. Cell Dev. Biol.* **12**, 463-518.

Choi, C. K., Vicente-Manzanares, M., Zareno, J., Whitmore, L. A., Mogilner, A. and Horwitz, A. R. (2008). Actin and alpha-actinin orchestrate the assembly and maturation of nascent adhesions in a myosin II motor-independent manner. *Nat. Cell Biol.* **10**, 1039-1050.

Costes, S. V., Daelemans, D., Cho, E. H., Dobbin, Z., Pavlakis, G. and Lockett, S. (2004). Automatic and quantitative measurement of protein-protein colocalization in live cells. *Biophys. J.* **86**, 3993-4003.

Disatnik, M. H., Boutet, S. C., Lee, C. H., Mochly-Rosen, D. and Rando, T. A. (2002). Sequential activation of individual PKC isozymes in integrin-mediated muscle cell spreading: a role for MARCKS in an integrin signaling pathway. *J. Cell Sci.* **115**, 2151-2163.

Disatnik, M. H., Boutet, S. C., Pacio, W., Chan, A. Y., Ross, L. B., Lee, C. H. and Rando, T. A. (2004). The bi-directional translocation of MARCKS between membrane and cytosol regulates integrin-mediated muscle cell spreading. *J. Cell Sci.* **117**, 4469-4479.

Gatlin, J. C., Estrada-Bernal, A., Sanford, S. D. and Pfenninger, K. H. (2006). Myristoylated, alanine-rich C-kinase substrate phosphorylation regulates growth cone adhesion and pathfinding. *Mol. Biol. Cell* **17**, 5115-5130.

Gilhooly, E. M., Morse-Gaudio, M., Bianchi, L., Reinhart, L., Rose, D. P., Connolly, J. M., Reed, J. A. and Albino, A. P. (2001). Loss of expression of protein kinase C beta is a common phenomenon in human malignant melanoma: a result of transformation or differentiation? *Melanoma Res.* **11**, 355-369.

Gingell, D., Todd, I. and Bailey, J. (1985). Topography of cell-glass apposition revealed by total internal reflection fluorescence of volume markers. *J. Cell Biol.* **100**, 1334-1338.
Groves, J. T., Parthasarathy, R. and Forstner, M. B. (2008). Fluorescence imaging of membrane dynamics. *Annu. Rev. Biomed. Eng.* **10**, 311-338.
Hynes, R. O. (1992). Integrins: versatility, modulation, and signaling in cell adhesion. *Cell* **69**, 11-25.
Hynes, R. O. (2002). Integrins: bidirectional, allosteric signaling machines. *Cell* **110**, 673-687.
Iioka, H., Ueno, N. and Kinoshita, N. (2004). Essential role of MARCKS in cortical actin dynamics during gastrulation movements. *J. Cell Biol.* **164**, 169-174.
Izzard, C. S. and Lochner, L. R. (1976). Cell-to-substrate contacts in living fibroblasts: an interference reflexion study with an evaluation of the technique. *J. Cell Sci.* **21**, 129-159.
Katz, B. Z., Zamir, E., Bershadsky, A., Kam, Z., Yamada, K. M. and Geiger, B. (2000). Physical state of the extracellular matrix regulates the structure and molecular composition of cell-matrix adhesions. *Mol. Biol. Cell* **11**, 1047-1060.
Katz, F., Ellis, L. and Pfenninger, K. H. (1985). Nerve growth cones isolated from fetal rat brain. III. Calcium-dependent protein phosphorylation. *J. Neurosci.* **5**, 1402-1411.
Kaverina, I., Krylyshkina, O. and Small, J. V. (2002). Regulation of substrate adhesion dynamics during cell motility. *Int. J. Biochem. Cell Biol.* **34**, 746-761.
Kim, J., Blackshear, P. J., Johnson, J. D. and McLaughlin, S. (1994). Phosphorylation reverses the membrane association of peptides that correspond to the basic domains of MARCKS and neuromodulin. *Biophys. J.* **67**, 227-237.
Lee, J. and Jacobson, K. (1997). The composition and dynamics of cell-substratum adhesions in locomoting fish keratocytes. *J. Cell Sci.* **110**, 2833-2844.
Li, J., Zhu, Z. and Bao, Z. (1996). Role of MacMARCKS in integrin-dependent macrophage spreading and tyrosine phosphorylation of paxillin. *J. Biol. Chem.* **271**, 12985-12990.
Linnenbach, A. J., Huebner, K., Reddy, E. P., Herlyn, M., Parmiter, A. H., Nowell, P. C. and Koprowski, H. (1988). Structural alteration in the MYB protooncogene and deletion within the gene encoding alpha-type protein kinase C in human melanoma cell lines. *Proc. Natl. Acad. Sci. USA* **85**, 74-78.
Lock, J. G., Wehrle-Haller, B. and Stromblad, S. (2008). Cell-matrix adhesion complexes: master control machinery of cell migration. *Semin. Cancer Biol.* **18**, 65-76.
Lohof, A. M., Quillan, M., Dan, Y. and Poo, M. M. (1992). Asymmetric modulation of cytosolic cAMP activity induces growth cone turning. *J. Neurosci.* **12**, 1253-1261.
Luo, B. H. and Springer, T. A. (2006). Integrin structures and conformational signaling. *Curr. Opin. Cell Biol.* **18**, 579-586.
Manenti, S., Malecaze, F. and Darbon, J. M. (1997). The major myristoylated PKC substrate (MARCKS) is involved in cell spreading, tyrosine phosphorylation of paxillin, and focal contact formation. *FEBS Lett.* **419**, 95-98.
McLaughlin, S. and Aderem, A. (1995). The myristoyl-electrostatic switch: a modulator of reversible protein-membrane interactions. *Trends Biochem. Sci.* **20**, 272-276.
Mikule, K., Sunpaweravong, S., Gatlin, J. C. and Pfenninger, K. H. (2003). Eicosanoid activation of protein kinase C epsilon: involvement in growth cone repellent signaling. *J. Biol. Chem.* **278**, 21168-21177.
Myat, M. M., Anderson, S., Allen, L. A. and Aderem, A. (1997). MARCKS regulates membrane ruffling and cell spreading. *Curr. Biol.* **7**, 611-614.
Nobes, C. D. and Hall, A. (1995). Rho, rac, and cdc42 GTPases regulate the assembly of multimolecular focal complexes associated with actin stress fibers, lamellipodia, and filopodia. *Cell* **81**, 53-62.
Ohmori, S., Sakai, N., Shirai, Y., Yamamoto, H., Miyamoto, E., Shimizu, N. and Saito, N. (2000). Importance of protein kinase C targeting for the phosphorylation of its substrate, myristoylated alanine-rich C-kinase substrate. *J. Biol. Chem.* **275**, 26449-26457.
Oka, M. and Kikkawa, U. (2005). Protein kinase C in melanoma. *Cancer Metastasis Rev.* **24**, 287-300.
Oka, M., Ogita, K., Ando, H., Horikawa, T., Hayashibe, K., Saito, N., Kikkawa, U. and Ichihashi, M. (1996). Deletion of specific protein kinase C subspecies in human melanoma cells. *J. Cell Physiol.* **167**, 406-412.
Pankov, R., Cukierman, E., Katz, B. Z., Matsumoto, K., Lin, D. C., Lin, S., Hahn, C. and Yamada, K. M. (2000). Integrin dynamics and matrix assembly: tensin-dependent translocation of alpha(5)beta(1) integrins promotes early fibronectin fibrillogenesis. *J. Cell Biol.* **148**, 1075-1090.
Pfenninger, K. H. and Maylie-Pfenninger, M. F. (1981). Lectin labeling of sprouting neurons. I. Regional distribution of surface glycoconjugates. *J. Cell Biol.* **89**, 536-546.
Pinner, S. and Sahai, E. (2008). Imaging amoeboid cancer cell motility *in vivo*. *J. Microsc.* **231**, 441-445.
Rombouts, K., Lottini, B., Caligiuri, A., Francesco, L., Mello, T., Carloni, V., Marra, F. and Pinzani, M. (2008). MARCKS is a downstream effector in platelet-derived growth factor-induced cell motility in activated human hepatic stellate cells. *Exp. Cell Res.* **314**, 1444-1454.
Rosen, A., Keenan, K. F., Thelen, M., Nairn, A. C. and Aderem, A. (1990). Activation of protein kinase C results in the displacement of its myristoylated, alanine-rich substrate from punctate structures in macrophage filopodia. *J. Exp. Med.* **172**, 1211-1215.
Rottner, K., Hall, A. and Small, J. V. (1999). Interplay between Rac and Rho in the control of substrate contact dynamics. *Curr. Biol.* **9**, 640-648.
Sastry, S. K. and Burridge, K. (2000). Focal adhesions: a nexus for intracellular signaling and cytoskeletal dynamics. *Exp. Cell Res.* **261**, 25-36.
Sawano, A., Hama, H., Saito, N. and Miyawaki, A. (2002). Multicolor imaging of Ca(2+) and protein kinase C signals using novel epifluorescence microscopy. *Biophys. J.* **82**, 1076-1085.
Smilenov, L. B., Mikhailov, A., Pelham, R. J., Marcantonio, E. E. and Gundersen, G. G. (1999). Focal adhesion motility revealed in stationary fibroblasts. *Science* **286**, 1172-1174.
Spizz, G. and Blackshear, P. J. (2001). Overexpression of the myristoylated alanine-rich C-kinase substrate inhibits cell adhesion to extracellular matrix components. *J. Biol. Chem.* **276**, 32264-32273.
Swierczynski, S. L. and Blackshear, P. J. (1995). Membrane association of the myristoylated alanine-rich C kinase substrate (MARCKS) protein. Mutational analysis provides evidence for complex interactions. *J. Biol. Chem.* **270**, 13436-13445.
Szekeres, C. K., Trikha, M. and Honn, K. V. (2002). 12(S)-HETE, pleiotropic functions, multiple signaling pathways. *Adv. Exp. Med. Biol.* **507**, 509-515.
Takada, Y., Ye, X. and Simon, S. (2007). The integrins. *Genome Biol.* **8**, 215.
Tang, D. G., Tarrien, M., Dobrzynski, P. and Honn, K. V. (1995). Melanoma cell spreading on fibronectin induced by 12(S)-HETE involves both protein kinase C- and protein tyrosine kinase-dependent focal adhesion formation and tyrosine phosphorylation of focal adhesion kinase (pp125FAK). *J. Cell Physiol.* **165**, 291-306.
Thelen, M., Rosen, A., Nairn, A. C. and Aderem, A. (1991). Regulation by phosphorylation of reversible association of a myristoylated protein kinase C substrate with the plasma membrane. *Nature* **351**, 320-322.
Toomre, D. and Manstein, D. J. (2001). Lighting up the cell surface with evanescent wave microscopy. *Trends Cell Biol.* **11**, 298-303.
Toullec, D., Pianetti, P., Coste, H., Bellevergue, P., Grand-Perret, T., Ajakane, M., Baudet, V., Boissin, P., Boursier, E., Loriolle, F. et al. (1991). The bisindolylmaleimide GF 109203X is a potent and selective inhibitor of protein kinase C. *J. Biol. Chem.* **266**, 15771-15781.
Webb, D. J., Parsons, J. T. and Horwitz, A. F. (2002). Adhesion assembly, disassembly and turnover in migrating cells: over and over and over again. *Nat. Cell Biol.* **4**, E97-E100.
Webb, D. J., Brown, C. M. and Horwitz, A. F. (2003). Illuminating adhesion complexes in migrating cells: moving toward a bright future. *Curr. Opin. Cell Biol.* **15**, 614-620.
Woods, A. and Couchman, J. R. (1992). Protein kinase C involvement in focal adhesion formation. *J. Cell Sci.* **101**, 277-290.
Worth, D. C. and Parsons, M. (2008). Adhesion dynamics: mechanisms and measurements. *Int. J. Biochem. Cell Biol.* **40**, 2397-2409.
Zamir, E. and Geiger, B. (2001). Molecular complexity and dynamics of cell-matrix adhesions. *J. Cell Sci.* **114**, 3583-3590.